Design Fundamentals. McGraw-Hill Book Company, New York, 1982, 670 pp.

11. Standard Specifications for Highway Bridges. 13th ed., AASHTO, Washington, D.C., 1983.
12. G. Koenig, H. Weigler, H. Quitmann, and J. Stuelb. Nachtraegliche Verstaerkung von Spannbetonbruecken im Koppelfugenbereich mit bewehrten Betonlasten. Beton u. Stahlbetonbau, Heft 10, Oct. 1980, pp. 229-235.

Publication of this paper sponsored by Committee on Concrete Bridges.

Investigation of Broken Wires in Suspender Strands of I-470 Ohio River Bridge at Wheeling, West Virginia

JOHN M. KULICKI and BOYD P. STRAIN, JR.

ABSTRACT

On March 25, 1981, three wires were found to be broken on one of the suspender cables of the 780-ft, tied arch bridge over the Ohio River at Wheeling, West Virginia. The bridge had not yet been opened to traffic. Subsequent inspections showed that other cables also had broken wires and several had wires that were suspected of being broken. Wind-excited vibrations of the cables were found to be the cause of fretting fatigue that had led to the fractured wires--experimental studies confirmed analytical evaluations of the cable vibrations. An estimate was made of remaining fatigue life, which led to a decision to replace only those cables that were obviously affected. Plans were developed to replace cables by stretching them. This was accomplished through the use of a compression frame that surrounded an individual cable and gripped the cable so as to stretch it within the length of the frame, and free it from attachment brackets. New cables were installed that were equipped with a threaded stud extension so that a stud tightener could be utilized to tighten the cables in the confined space between the attachment bracket and the tie girder.

The Interstate 470 (I-470) Bridge (No. 2494) which crosses the Ohio River at Wheeling, West Virginia, is a 780-ft-long, tied arch designed for the West Virginia Department of Highways by a firm of consulting engineers. An elevation view of the arch span is shown in Figure 1 and a general view of the bridge is shown in Figure 2. Steel erection began on July 27, 1977, the arch ribs and girders were completed on November 7, all hangers and cables were in place by December 1, the structure was swung free of falsework on December 31, and all steelwork was completed by May 8 of the following year. Steelwork painting was completed in July 1978, and the concrete deck was placed from July to September 1980. Placement of the latex road and concrete roadway wearing surface began in March 1981 when work was stopped for this investigation. At that time, the eastern half of the eastbound lanes had the latex wearing surface in place.

The suspenders are sets of four, 2.25-in. bridge strands with a minimum breaking strength of 310 t each and a Class A zinc coating. Data provided by the U.S. Steel Corporation, the original supplier of the strands, indicated that the strands were composed of a wire core, approximately 0.75 in. in diameter and containing 19 wires, covered with successive alternate layers of 15, 21, 27, and 33 wires (a total of 115 wires), of which 91 are 0.188 in. in diameter and 24 are smaller core or filler wires. Suspender vibrations had been observed during the construction period, but vibrations of some extent are common to cable use and installations, and were not officially reported.

On March 25, 1981, three wires of the southeast strand at Panel Point T8 downstream (DS) were observed by inspectors of the West Virginia Department of Highways to have been broken and unwound upward along the strand. Figure 3 shows the conditions at Panel Point T8 DS observed on March 31, 1981. (This photograph also shows some of the strand attachment details that are shown in Figure 4.) Note that there are no collars or other restrainers detailed on the bridge.

Wooden wedges, which are evident in Figure 3, were driven between the strands and the lower attachment assemblies, and an investigation of the extent and cause of the broken wires was ordered by the West Virginia Department of Highways. The wooden

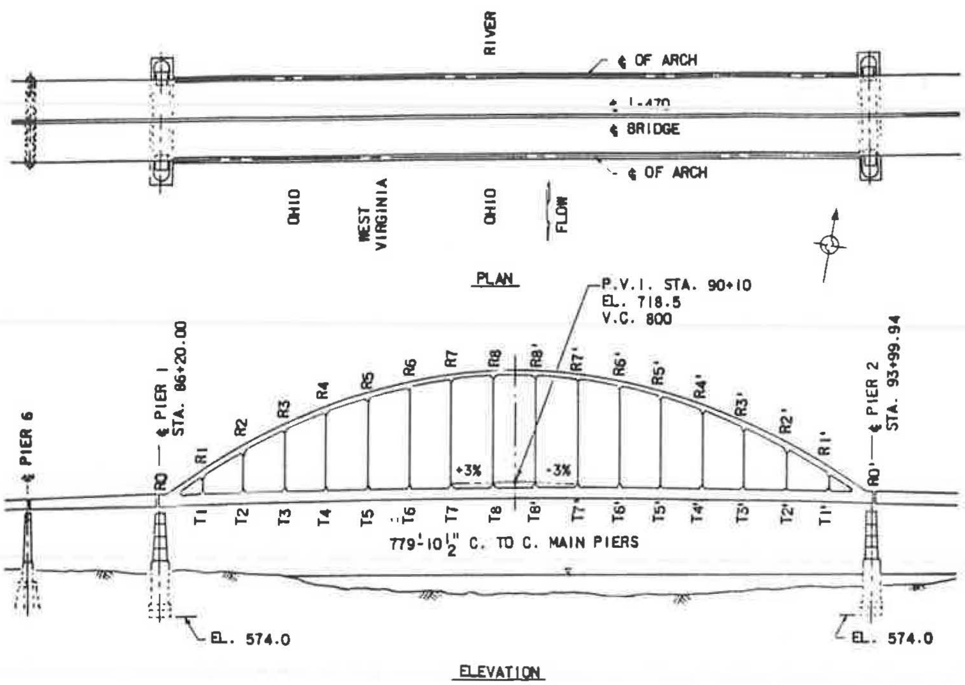

FIGURE 1 General plan and elevation of arch span.

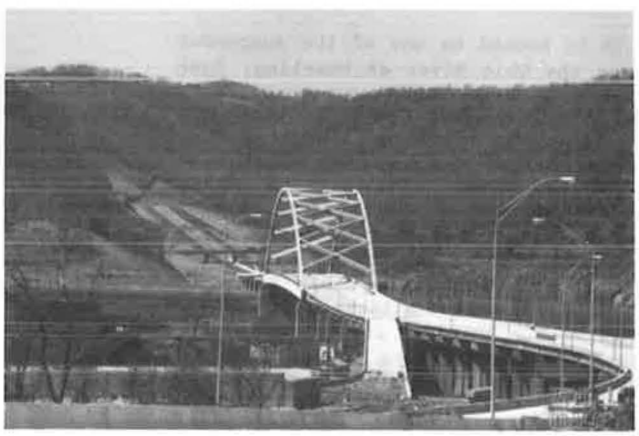

FIGURE 2 General view of bridge (looking northwest).

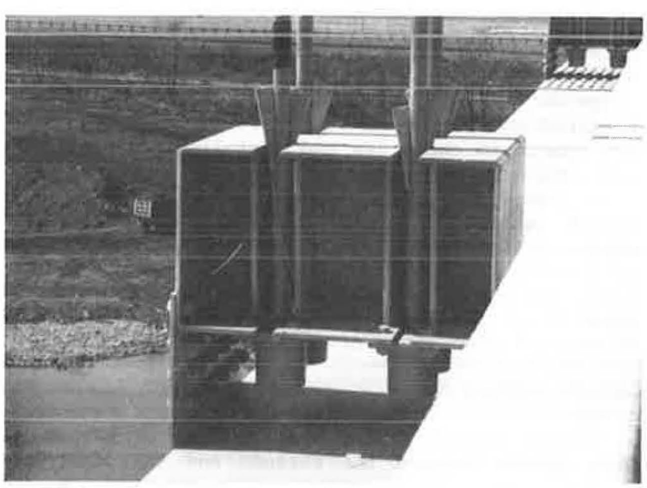

FIGURE 3 T8-DS original detail (looking west) and showing wood wedges used to inhibit vibration.

wedges had a significant damping effect on the strand vibration, reducing the amplitude so that movement was hardly discernible by eye. A small movement could still be felt, however.

Comments were solicited from field personnel relative to strand vibrations during construction and the following information was obtained:

1. Strands vibrated under most mild wind conditions.
2. Vibrations were easily observable from some distance.
3. The four strands at each panel point did not vibrate in unison.

A two-phase approach was taken to study the strand vibration problem and determine its significance. The work phases and individual tasks are as follows:

PHASE I

1. Visually inspect (a) the full length of all strands, sockets, and connection areas and record any broken or cracked wires and other abnormalities; (b) the exterior of the top flange of the tie box-girder and those adjacent portions of the web plates that can be seen from the top flange for cracks; and (c) additional portions of the structure, as necessary, as the investigation proceeds.
2. Remove a portion of each of the three broken wires at Panel Point T8 DS as well as any other broken wires that are discovered, and deliver them to Lehigh University for examination of the fracture surfaces.
3. Determine the possibility of finding interior wire fractures using nondestructive inspection methods. If found practical, inspect the strands for interior-wire fractures.
4. Perform any structural analyses, studies, or investigations that may be required to determine the reasons for the failure of the wires, and develop repair requirements and methods.
5. Develop recommendations regarding placing the

bridge in service. Recommend details to eliminate the cause, or causes, of the wire failures. Prepare preliminary cost estimates.

PHASE II

1. If major corrective work is required, develop plans, procedures, specifications, and estimates to perform the work.

2. If required by the Department, provide inspection of construction during the repair process.

FIELD INSPECTION FINDINGS

At various times during April and May of 1981, Modjeski and Masters made detailed inspections of the strands, strand connections, and top flanges of

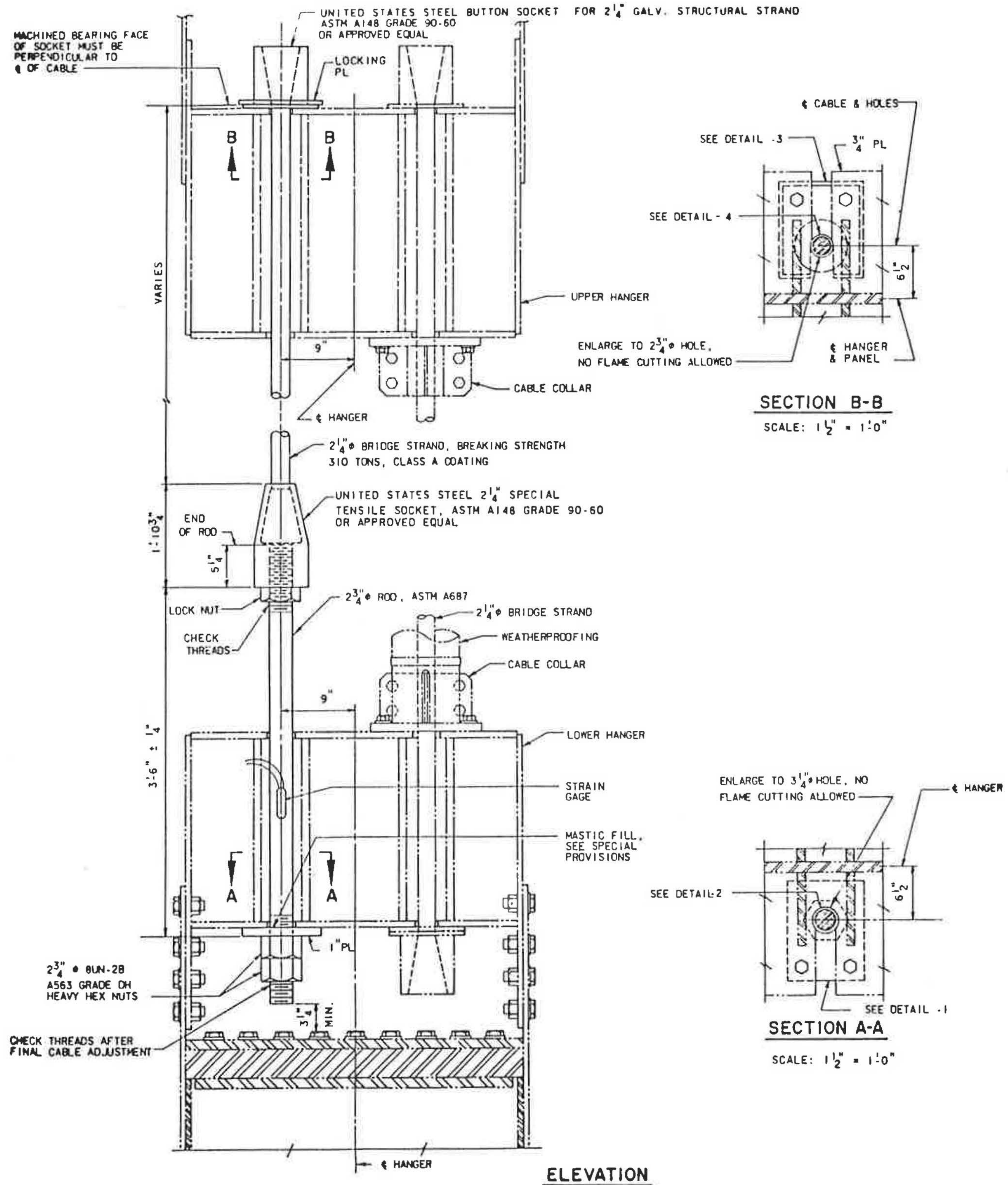

FIGURE 4 General retrofit details.

the tie girders. Six broken wires were found in individual strands, and two other wires were suspected of being broken by virtue of slight deviations of their position in the wire bundle, but no fracture surfaces were observed. No significance was found in the fact that all wire breaks took place on the downstream rib and tie. These wires are located as given in Table 1. Wires 5, 7, and 8 could not be readily removed from the strand. Wire 6 was removed but not tested because (a) the overall appearance was quite similar to that of Wires 1, 2, and 4; (b) the fracture surface was quite corroded compared to that of the other samples; and (c) an oral report of electron microscope studies (in progress when Wire 6 was found) indicated that the first four samples were quite similar.

TABLE 1 Wire Data

Wire	Suspender	Strand	Condition	Sample Taken	Sample Tested
1	T8 DS	SE	Broken	Yes	Yes
2	T8 DS	SE	Broken	Yes	Yes
3	T8 DS	SE	Broken	Yes	Yes
4	R5'DS	NW	Broken	Yes	Yes
5	R5'DS	NE	Broken	No	–
6	R7 DS	NW	Broken	Yes	No
7	T7 DS	SW	Suspect	No	–
8	T7 DS	SW	Suspect	No	–

Note: SE = southeast, NW = northwest, SW = southwest, NE = northeast, and DS = downstream.

Sketches were made of the five samples of wire taken from the bridge. A typical sketch is shown in Figure 5. All five samples had a "brown-colored" area or "possible wear" mark similar to that noted in Figure 5. Traces of the field coat of paint that is visible on the wire indicated that the "brown" or "wear" mark was on the outside of the strand (i.e., away from the web of the attachment detail). Field inspection indicated that each broken wire was a rear wire and would have been in contact with the closed end of the slot on the bearing plate (i.e., there was no perceptible clearance between wire and plate). (See Figure 4 for location of bearing plate.)

Careful inspection of the suspender assemblies showed that in all but 31 of 256 possible locations, the strands appeared to be touching the bearing plates. This condition resulted in fretting fatigue during strand vibrations such as those observed before the wooden wedges were put in place. Photographs were taken to document the observed conditions; a typical set of photographs is shown in Figure 6. The apparent touching of strands on bearing plates is shown in the mirror in each photograph used to observe the conditions on the rear face of the individual strands. Also, measurements were made of the observed position of each strand as it passed through the slots on the flanges of the suspender attachment detail; a typical set of measurements is shown in Figure 7.

SUMMARY OF FRACTOGRAPHIC FINDINGS

Wires 1-4 were sent to Fisher, Fang, and Associates, Inc., in Bethlehem, Pennsylvania, to be studied under the scanning electron microscope at Lehigh University. Studies were performed by Dr. Alan Pense and reviewed by Dr. John W. Fisher (1). The report by Fisher, Fang, and Associates, Inc., is summarized as follows:

1. All four samples of wire showed evidence of fatigue cracking propagating through a significant portion of the cross-section at the fracture.

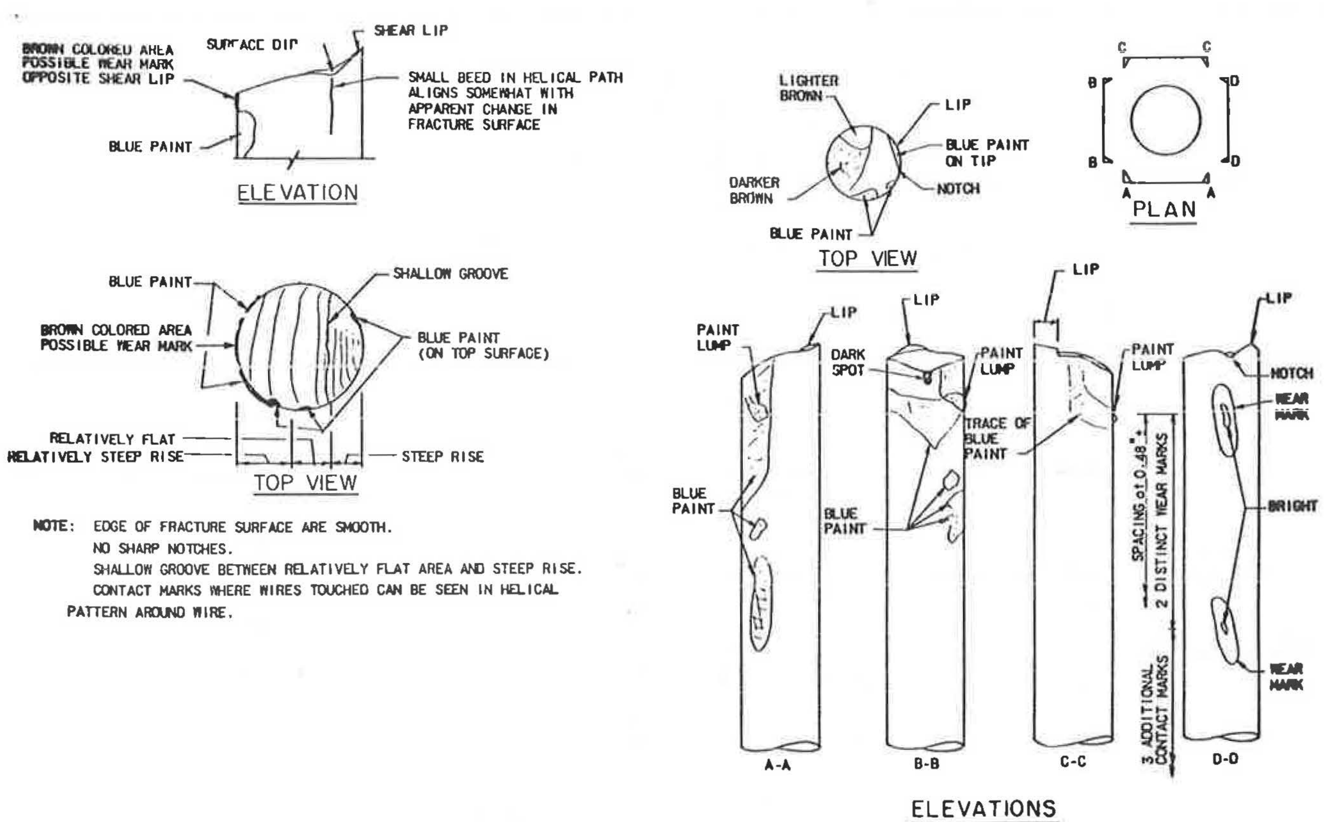

FIGURE 5 Surface characteristics of wire from TS-DS-SE—Wire 2.

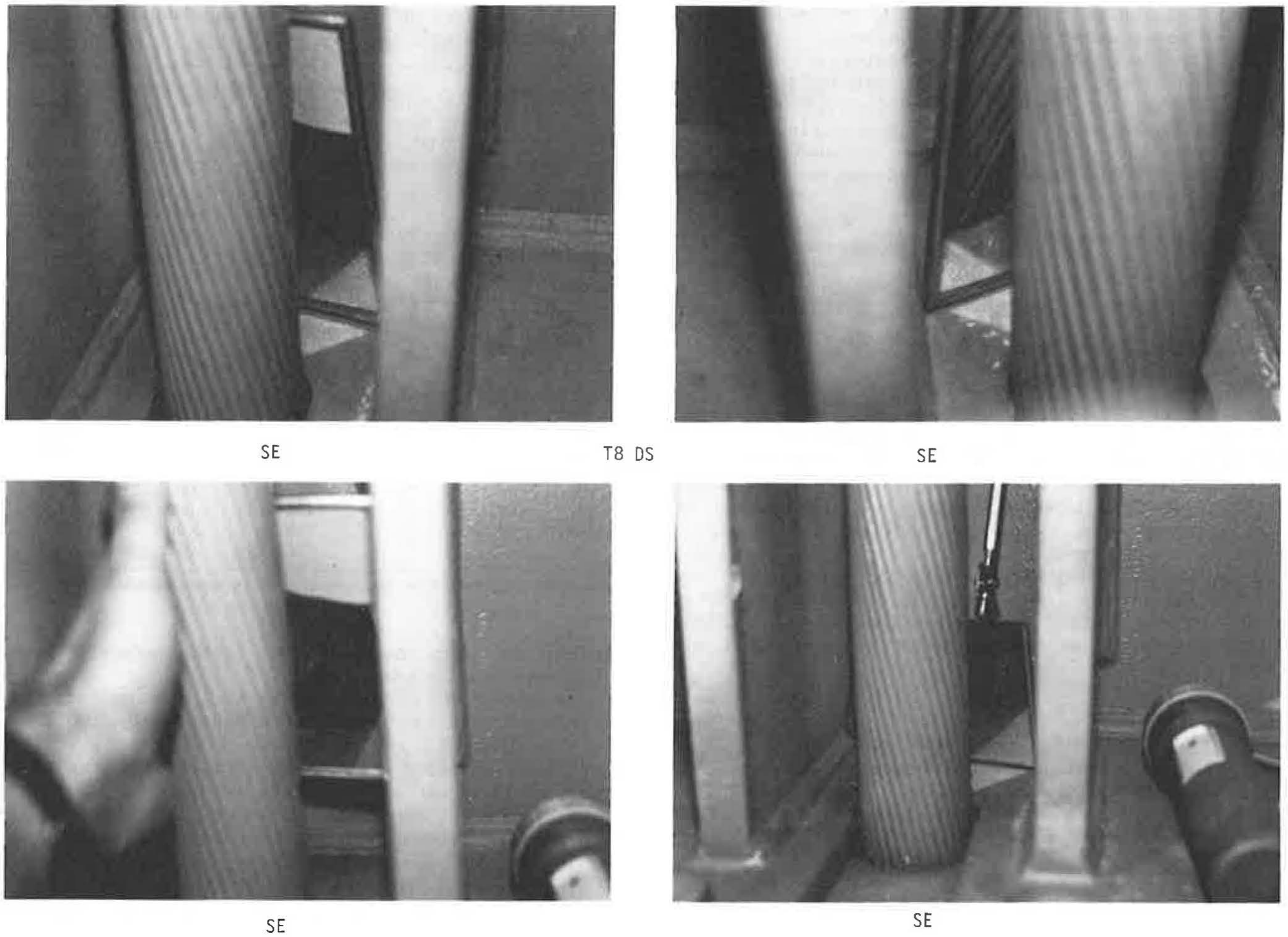

FIGURE 6 Typical inspection findings.

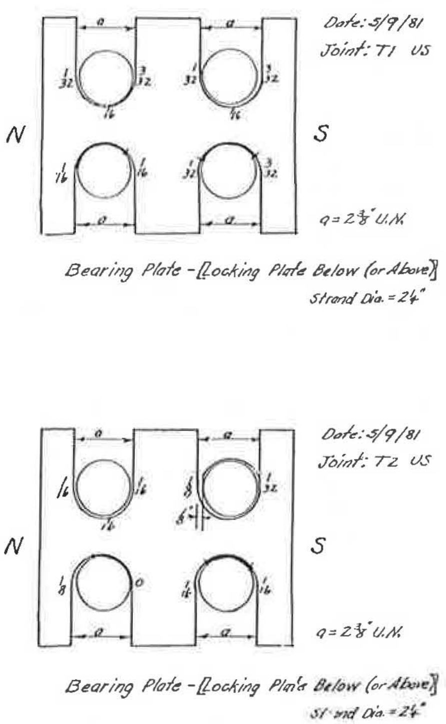

FIGURE 7 Typical inspection measurements.

2. The fatigue cracks began at the brown or wear spots identified in the sketches of wires (see Figure 5).

3. The brown or wear mark appears to be caused by numerous abrasive occurrences, rather than by a single event.

4. There were visible paint specks on the fracture surface. There was fatigue and/or corrosion under the paint specks, indicating that the areas under the paint specks were not pre-existing flaws at which fatigue started, and that the paint was apparently deposited as the wires broke and the projecting ends struck a painted surface.

5. The socketing process caused no metallurgical degradation of wires.

6. A tensile test performed on Wire 1 showed a yield point of 185 ksi, a tensile strength of 234 ksi, a 48 percent reduction in area, and a 14 percent elongation in 1 in.--all of which are acceptable values.

STRAND VIBRATION FIELD TESTS

Introduction

Battelle Memorial Institute was engaged to mount an accelerometer on various strands to determine the following:

1. The first-mode frequencies of several sets of strands, which would be used to compute strand tension.

2. Frequencies of vibration for comparison with computed modes under various wind speeds.
3. Wind-induced vibration characteristics.
4. The amount of damping provided by the as-designed system and the system modified by the addition of wooden wedges. (The wedge-modified damping values were thought to be of value because the damping caused by the wedges appeared to be enough to still the vibration.)

A summary of the report (2) is presented in the following sections.

Experimental Procedure

The sixteen strands selected as representative are the four sets of four each at R8, R8', R5', and R3'. All strands examined were on the downstream side of the bridge. The R8 and R8' sets of suspenders are nominally identical under full dead load, and only slightly different with the partial application of the latex-modified concrete wearing surface previously noted. From the nominal tension, lengths, and mass, the theoretical natural frequencies for lateral vibrations in the strands can be computed as shown in the section entitled "Analysis of Cable Vibrations." The calculated natural frequencies are given in Table 2.

TABLE 2 Calculated First-Mode Natural Frequencies of Representative Strands

Suspender	Strand Length[a] (ft)	Tension (kips per strand)	Natural Frequency (Hz)
3'	64.77	118	4.80
5'	97.23	115	3.11
8	119.18	113	2.48

[a]From the fabricator's shop drawings, between bearing faces of sockets.

Determination of Natural Frequencies

An accelerometer was clamped to the midpoint of the strand such that its measurement axis was horizontal. The midpoint was chosen to maximize the acceleration attributable to the first or fundamental mode of vibration. The strand was manually pushed and pulled in a periodic way that approximately corresponded with the observed natural frequency. After building up the amplitude of the strand, it was released and allowed to vibrate freely for approximately 2 min. Generally, the strand vibrated in the first mode with little contamination from the higher modes. In some cases, the third mode contributed sufficiently to be evident in the recordings; however, even in these cases, the first mode was clearly discernible. The peak-to-peak amplitude of Strand R8' SW resulting from manual excitation was calculated as 1.7 in. On-site measurements indicated an estimated amplitude of 1.5 in.

Results

Table 3 gives the measured fundamental frequencies of vibration of the 16 strands. Strand tensions shown in the table were calculated by using the relationships shown in the section entitled "Fundamentals of Vortex Shedding Excitation." These values are for individual strands. Because they were evaluated experimentally, the total load for the four strands

TABLE 3 Measured Natural Frequencies and Damping of Representative Strands

Strand	Length (ft)	Natural Frequency (Hz)	Dead Load Tension (kips)	Damping Constant[a] With Wedges	Without Wedges
R8					
NE	119.18	2.33	97	.0005	(0)
NW	119.18	2.25	91	.0005	(0)
SE	119.18	2.25	91	.0011	(0)
SW	119.18	2.28	93	.0013	(0)
R8'					
NE	119.18	2.22	88	(0)	.0005
NW	119.18	2.41	104	.0005	.0003
SE	119.18	2.26	93	.0005	(0)
SW	119.18	2.03	74	.0004	(0)
R5'					
NE	97.23	3.25	126	.0006	.0003
NW	97.23	3.47	144	.0006	.0002
SE	97.23	3.40	138	.0009	.0003
SW	97.23	3.33	132	.0006	.0001
R3'					
NE	64.77	4.26	93	.0005	.0004
NW	64.77	5.05	133	.0005	.0004
SE	64.77	5.18	140	.0005	.0003
SW	64.77	4.93	126	.0005	.0006

[a]Parentheses indicate that damping value was too small to estimate reliably.

forming one suspender does not agree exactly with the theoretical loads.

The attempts to determine the damping of the strands without the wedges were thwarted by two factors: the damping is low and, in some cases, random excitation caused by wind was sufficiently large to cause an increase in amplitude during the time interval recorded. Even the attempts to determine the damping with wedges were not completely satisfactory for the same reasons. Nevertheless, an estimated damping factor, which follows, is given in Table 3 for each of the 16 strands, with and without wedges:

$$\zeta = \text{Log}_e\ (R)/2\pi N \qquad (1)$$

where R is the ratio of displacements at cycle number N1 and N2, and N is N2 - N1 (absolute value).

ANALYSIS OF CABLE VIBRATIONS

Discussions throughout this section will be in the context of air moving around an obstruction that is basically circular in cross-section.

The design dead loads calculated by the original designer were reviewed, found to be correct, and then revised to reflect the condition of the bridge when work stopped. The resulting strand tensions, in kips, are given in Table 4. (Note that the average values of the symmetric panel points were used in the analysis presented herein.)

Fundamentals of Vortex Shedding Excitation

When air passes by a circular shape, the air flow divides to pass around the obstruction. The activity generated in the wake of the obstruction can be related to the Reynolds Number

$$R_e = Vd\rho/\mu \qquad (2)$$

where

V = velocity (ft/sec),
d = characteristic dimension (ft),
ρ = mass density (lb-sec^2/ft^4), and
μ = dynamic viscosity (lb-sec/ft^2).

TABLE 4 Strand Tensions

Suspender No.	Tension per Strand (kips)	Suspender No.	Tension per Strand (kips)
1	118	8′	113
2	102	7′	96
3	117	6′	114
4	93	5′	115
5	115	4′	93
6	114	3′	118
7	96	2′	102
8	113	1′	119

Chi has categorized wake responses ranging from Reynolds Numbers 1 to 3.5 x 10^6 (3,4). The most practical cases (temperatures greater than 0°F and wind speeds less than 50 mph) are in the subcritical flow range. In this regime, the wake consists of regularly spaced alternating vortices similar to the "Von Karman vortex street" that occurs at lower Reynolds Numbers, except that the fluid action in the vortices may be turbulent, and the frequency of vortex shedding is given by

$$f_s = S_t V/d \tag{3}$$

where

V = wind velocity (ft/sec),
d = diameter (ft),
S_t = Strouhal number (unitless), and
f_s = frequency of vortex shedding (Hz).

For a circular cylinder, the Strouhal number is relatively constant at approximately 0.20 for the Reynolds Numbers under consideration, although experimental results have ranged from about 0.185 to 0.22 (5,6).

The potential for large amplitude vibrations exists when a forcing function drives a structural component at a frequency close to one of its natural frequencies (i.e., resonance) and when there is very little damping. Strands, such as the one on the I-470 Bridge, have little natural damping as evidenced by the low value of damping obtained in the field studies. Thus, the basic principle underlying an investigation of vortex-shedding-induced vibrations is to equate the vortex shedding frequency equation to an equation for natural frequencies and solve for critical wind speeds. Theoretically, this yields a discrete wind speed for each natural frequency.

In actuality, a phenomenon called "lock-in" occurs in which the vortex shedding and structural vibration interact with each other. The result is that the structure vibrates in a given mode for a range of wind speeds generally regarded as being from the critical wind speed for that mode to approximately 140 percent of the critical wind speed (7). During this interval of wind speeds, the frequency of vortex shedding is controlled by the structural frequency, rather than the wind speed.

The simplest representation of a vibrating cable is obtained by neglecting the bending stiffness and treating the cable as a string. The frequencies of vibration are given by the following equation:

$$f_n = (n/2L)[(T/m)^{1/2}] \tag{4}$$

where

n = mode number,
f = frequency (Hz),
L = length (ft),
T = load (kips), and
m = mass per unit length (kips-sec²/ft²).

If the bending rigidity is included, the following differential equation results:

$$[EI(\partial^4 y/\partial x^4)] - [T(\partial^2 y/\partial x^2)] + [m(\partial^2 y/\partial t^2)] = 0 \tag{5}$$

This equation has been solved by Modjeski and Masters (8) and others, including Chi (3,4). For the applicable case of fixed ends, there is no simple solution; rather, a trial and error process results. By generally using the nomenclature in reports by Chi (3,4), the following equations result:

$$\mathrm{Cosh}\beta_n \, \mathrm{Cos}\alpha_n + [(\alpha_n^2-\beta_n^2)/2\alpha_n\beta_n] \, \mathrm{Sinh}\beta_n \, \mathrm{Sin}\alpha_n = 1.0 \tag{6}$$

$$\alpha_n^2 = (p/2)\,|-1 + \{1 + [(4Q/p^2)]\}^{1/2}| \tag{7}$$

$$\beta_n^2 = (P/2)\,|1 + \{1 + [(4Q/p^2)]\}^{1/2}| \tag{8}$$

$$Q = m\omega_n^2 L^4/EI \tag{9}$$

$$P = TL^2/EI \tag{10}$$

where

ω_n = frequency (rads/sec),
I = moment of inertia (in.²/ft²), and
E = Young's modulus (ksi).

The solution, given M, E, I, T, and L, is to assume trial values of n until Equation 6 is satisfied. The only practical way to solve Equation 5 is by trial-and-error calculations or by using graphs developed by Chi. A computer program was written for this investigation.

Equation 6 requires a value for the moment of inertia of the cable. For the I-470 Bridge, this value could reasonably be expected to lie between a solid cylinder 2.25 in. in diameter (I = 1.258 in.⁴) and the sum of the moments of inertia of the 91 large wires (I = 0.0056 in.⁴), depending on the interwire shear which, in turn, depends on the wire-to-wire transverse pressure. The transverse pressure varies with the amount of tension and the extent of "birdcaging" caused by the vibration. Not surprisingly, tests on stranded transmission wire by Scanlan and Swart (9) indicated that the flexural stiffness of the stranded wire varied along the length of the wire, being higher near regions of lateral confinement, and that the effective rigidity varied from 0.1 to 0.5 of that of a solid shape.

Frequencies were computed using 10, 30, 50, and 100 percent of the moment of inertia of a solid shape. The effect of bending stiffness increased with higher modes, and was more significant for the shorter strands.

The experimental results were used to provide some insight into the amount of bending rigidity present. If there were no bending rigidity, the frequencies would form an arithmetical progression (i.e., 1, 2, 3, 4 ...) as shown by Equation 4. A plot of mode number versus frequency would be a straight line. Equation 6 becomes increasingly nonlinear for a given strand as the bending rigidity increases. Figure 8 shows the degree of nonlinearity [i.e., $f_n/(n \times f_1)$] associated with each of the assumed percentages of solid rigidity. Also plotted are various ratios of peak frequency to multiples of measured frequencies. These data are neither numerous enough nor of high enough modes (large nonlinearity regions) to make strong quantitative conclusions, but they indicate a trend toward effective rigidities

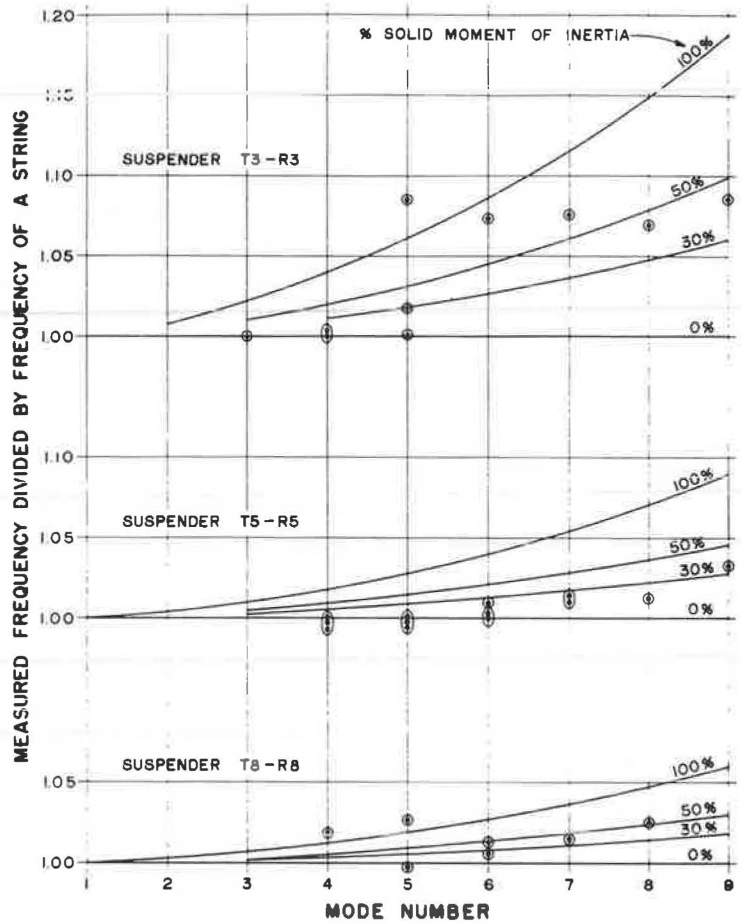

FIGURE 8 Effect of strand bending stiffness on frequency.

such as those encountered by Scanlan and Swart (i.e., varying from 10 to 50 percent effective stiffness along the length of the cable), which means an average value of less than 50 percent. An average value of 30 percent effective stiffness was used in developing the critical wind speeds given in Table 5. Given that the Strouhal Number could vary by 10 percent, a more involved evaluation of effective strand bending stiffness would have no practical significance for this study.

Correlation of Measured and Computed Wind Speeds

The wind during the test periods had noticeable gusting and excited several modes of strand vibra-

TABLE 5 Critical Wind Speeds

Mode No.	Winds Speed (mph) by Strand Identification							
	T1-R1	T2-R2	T3-R3	T4-R4	T4-R5	T6-R6	T7-R7	T8-R8
1	13	4	3	2	2	2	2	2
2	28	9	6	4	4	4	3	3
3	44	14	9	6	6	5	5	5
4	62	18	12	9	8	7	6	6
5	84	23	16	11	10	9	8	8
6	108	29	19	13	12	11	9	10
7	136	34	22	15	14	13	11	11
8	167	40	26	18	16	14	13	13
9	201	46	29	20	18	16	14	15
10	239	53	33	23	21	18	16	16
11	281	60	37	25	23	20	17	18
12	326	67	41	28	25	22	19	20
13	375	75	45	30	27	24	21	22
14	428	84	49	33	30	26	23	23
15	484	92	53	36	32	28	25	25
16	544	102	58	39	34	30	26	27
17	608	111	63	42	37	33	28	29
18	675	122	68	45	40	35	30	31
19	746	133	73	48	42	37	32	33
20	821	144	78	52	45	39	34	35

Note: In this table, strand I = 0.3774 and E = 24,000.

tion. The recording anemometer set up on the bridge measured only average data for 1-min intervals and did not function reliably. Readings from the anemometer on Wheeling Island, which is several miles away, were obtained but did not seem to correlate to winds observed at the bridge site. The result is that the only available, reliable measurements of wind speed were those made with a hand-held anemometer (pressure plate type). Nevertheless, the following correlations between calculated and measured wind speeds were possible:

1. The 3rd, 4th, and 5th modes of Strand 8 DS-NE were reasonably represented in field data, with the 3rd and 4th modes dominant when the wind speed was about 5 mph. Table 5 gives the computed wind speeds at 5, 6, and 8 mph, respectively, for the 3rd, 4th, and 5th modes.
2. The 7th mode was dominant in the field data with some 6th and 8th mode participation for Strand 8 DS-NE when the wind speed was 12-15 mph. The computed wind speeds are 10, 11, and 13 mph, respectively, for the 6th, 7th, and 8th modes.
3. Strand 5' DS-SE was observed in winds ranging from 10-15 mph. Modal representation in the field data included the 4th through 7th modes. The corresponding computed wind speeds are 8, 10, 12, and 14 mph, respectively.
4. Strand 3' DS-NE was also observed in 10-15 mph winds. Field data indicate that the 3rd to 5th modes were active. Corresponding computed wind speeds were 9, 12, and 16 mph, respectively.

In considering the uncertainties in the Strouhal Number, the effective strand rigidity, and the measured wind speed, as well as the fact that individual strands in a set of four at a panel point had slightly different frequencies (largely because of unequal tensions), the computed and measured critical wind speeds are in good agreement.

Strand Vibration Amplitudes and Tensions

Analytic procedures described by Chi (4) were also used to estimate vibration amplitudes and strand tensions. This procedure, as modified by the authors, consists of the following equations:

$$\phi_n(X) = [A_n \operatorname{Sin}\alpha_n(X/L)] + [B_n \operatorname{Cos}\alpha_n(X/L)] + [C_n \operatorname{Sinh}\beta_n(X/L)] + [D_n \operatorname{Cosh}\beta_n(X/L)] \quad (11)$$

where

$$A_n = 1.0 \quad (12)$$

$$B_n = (\alpha_n \operatorname{Sinh}\beta_n - \beta_n \operatorname{Sin}\alpha_n) \div [\beta_n(\operatorname{Cos}\alpha_n - \operatorname{Cosh}\beta_n)] \quad (13)$$

$$C_n = -\alpha_n/\beta_n \quad (14)$$

$$D_n = -B_n \quad (15)$$

$$Y(x,t) = \sum_n Y_n(x,t) = \sum_n \phi_n(x)\ (G_{1n} \operatorname{Sin}\omega_s t + G_{2n} \operatorname{Cos}\omega_s t) \quad (16)$$

In Equation 16, ω_s is the frequency of vortex shedding. A reasonable simplification for wind-induced, essentially resonant, vibration is to assume that the vibration consists of one mode shape and that $\omega_n = \omega_s$. Since ϕ is a shape function and, therefore, has a maximum value of 1.0, G_{2n} is 0 when $\omega_n = \omega_s$(4), and $\operatorname{Sin}\omega_s t$ has a maximum value of 1.0, so that:

$$Y_{max} \sim G_{1n} \quad (17)$$

For the case of $\omega_n = \omega_s$, the equation for G_{1n} reduces to

$$G_{1n} = (T_{on}/M_n)\ (1/2\zeta_n\omega_n^2) \quad (18)$$

$$M_n = \int_0^L m\phi_n(x)^2 dx \quad (19)$$

$$T_{on} = (1/2)\rho_a d V_{cr}^2 C_L \int_0^L \phi_n(x) dx \quad (20)$$

where

ζ = damping factor,
ρ_a = mass density of air, and
C_L = lift coefficient taken as 1.20.

Equations 19 and 20 were evaluated by using numerical methods.

Maximum amplitudes computed by using Equations 11-20 are shown in Table 6 for a damping factor of 0.0003, which is representative of the values obtained during the field tests. The single amplitudes shown in Table 6 are approximately one-half of the double amplitudes observed in the field, which were approximately 0.75 in. Although this result is encouraging, Equation 18 shows that the maximum computed amplitude is a linear function of the damping factor, a factor found with limited accuracy during the field tests, and seldom known with reliability during design. Similarly, the lift coefficient has been assumed to be a constant and it, too, varies with frequency.

Tension may be computed by differentiating Equation 16 twice to compute curvature. The magnitude of the curvature is also a linear function of damping and is dependent on the value chosen for effective bending stiffness of the strand. The local bending stiffness near points of lateral restraint (i.e., the sockets) results in local stresses that are higher than those that would be obtained by using the average bending stiffness. The stresses reported herein are based on curvatures computed using an average stiffness of 30 percent of a solid and then multiplied by the ratio of an assumed locally higher bending stiffness to the average bending stiffness. For comparison, Table 7 shows stresses based on 30 percent average stiffness, and local stiffness of 30, 60, and 100 percent of a solid. The 60 percent stiffness was chosen as the most realistic on the basis of experimental work by Scanlan and Swart that indicated effective stiffness of up to 50 percent of a solid and the assumption that the socket is more effective in providing lateral restraint than transmission wire fittings.

In considering the magnitude of computed stresses, and therefore stress ranges, it is important to bear in mind that the computed results depend on the chosen values of damping, local stiffness, and average stiffness. Values have been used that were believed to be representative and documentable to the extent possible, but they are still only assumptions.

Analysis of Fatigue

There are three stages of fatigue life: initiation, propagation, and instability. Basically, only the first two stages are important in this investigation.

Much of the available information on fatigue of wire and fabricated strands deals with wire, rather than strand. There is a limited body of information on wire fatigue and this has been reviewed by Chi (4). Much of the same information had been obtained for this investigation before Chi's report was available, and, fortuitously, has been analyzed and critiqued by Chi. Comments in this section of this report are based largely on Chi's analysis of the available data.

When clean, smooth wire is tested in fatigue, it is generally found to have a reasonably high fatigue life. It is also found that the majority of the fatigue life is represented by the crack initiation phase, with relatively little life in the crack propagation phase (i.e., once cracks have been initiated, they propagate quickly). In the case of a helically wound strand, fatigue cracks usually start at mechanical notches caused by point contact between

TABLE 6 Strand Vibration Amplitudes from Analytic Solution

	Strand Identification							
Specifications	T1-R1	T2-R2	T3-R3	T4-R4	T5-R5	T6-R6	T7-R7	T8-R8
Tension (kips)	474	409	470	372	459	455	383	442
Length (ft)	16.1	42.0	64.2	82.1	97.2	108.1	144.8	119.2
Mode no. (in.)								
1	.45	.46	.46	.46	.46	.46	.46	.46
2	.44	.45	.46	.46	.46	.46	.46	.46
3	.42	.45	.45	.45	.46	.46	.46	.46
4	.40	.44	.45	.45	.45	.45	.45	.46
5	.39	.44	.45	.45	.45	.45	.45	.45
6	.37	.43	.44	.45	.45	.45	.45	.45
7	.37	.42	.44	.45	.45	.45	.45	.45
8	.36	.41	.44	.44	.45	.45	.45	.45
9	.35	.41	.43	.44	.44	.45	.45	.45
10	.35	.40	.43	.43	.44	.44	.44	.45
11	.34	.39	.42	.43	.44	.44	.44	.44
12	.34	.39	.42	.43	.44	.44	.44	.44
13	.34	.38	.41	.42	.43	.44	.44	.44
14	.34	.38	.41	.42	.43	.44	44	.44
15	.33	.37	.41	.41	.43	.43	.43	.44
16	.33	.37	.40	.41	.43	.43	.43	.43
17	.33	.37	.40	.41	.42	.43	.43	.43
18	.33	.36	.39	.40	.42	.42	.42	.43
19	.33	.36	.39	.40	.42	.42	.42	.43
20	.33	.36	.39	.39	.41	.42	.42	.42

Note: In this table, the assumed strand I value is 0.3774, the damping value is .0003, and the moment of inertia used to calculate local bending stress is 0.7548.

TABLE 7 Strand Bending Stresses at Socket (ksi)

Mode	Strand Identification							
No.	T1-R1	T2-R2	T3-R3	T4-R4	T5-R5	T6-R6	T7-R7	T8-R8
Assuming I = 30 Percent of That of Solid Bar								
1	29	9	6	4	4	4	3	3
2	62	19	13	9	8	7	6	7
3	>100	29	20	14	13	11	10	10
4	>100	40	27	18	17	15	13	14
5	>100	52	34	23	21	19	16	17
6	>100	64	41	28	26	23	20	21
7	>100	78	49	33	30	27	23	24
8	>100	93	57	39	35	31	27	28
9	>100	>100	65	44	40	35	30	31
10	>100	>100	74	50	44	39	34	35
Assuming I = 60 Percent of That of Solid Bar								
1	58	19	13	9	8	7	6	7
2	>100	38	26	18	17	15	13	13
3	>100	58	39	27	25	23	19	20
4	>100	80	53	37	34	30	26	27
5	>100	>100	67	46	43	38	33	34
6	>100	>100	82	56	51	46	40	41
7	>100	>100	97	67	61	54	47	48
8	>100	>100	>100	77	70	62	54	55
9	>100	>100	>100	88	79	70	61	62
10	>100	>100	>100	>100	89	79	68	70
Assuming I = 100 Percent of That of Solid Bar								
1	97	31	22	15	14	12	11	11
2	>100	64	43	30	28	25	22	23
3	>100	97	66	45	42	38	32	34
4	>100	>100	88	61	56	50	43	45
5	>100	>100	>100	77	71	63	55	57
6	>100	>100	>100	93	86	76	66	69
7	>100	>100	>100	>100	>100	90	78	81
8	>100	>100	>100	>100	>100	>100	89	93
9	>100	>100	>100	>100	>100	>100	>100	>100
10	>100	>100	>100	>100	>100	>100	>100	>100

individual wires. This reduces the crack initiation phase of fatigue life.

There is even less knowledge of the fatigue life of strand than of wire. While the mechanism of fretting is a factor in strand fatigue, there is apparently no accepted analytical model for predicting cycles-to-failure under a given stress range. However, some of the experimental work reviewed by Chi indicates the order of magnitude of strand fatigue life. For example,

1. Reemsnyder (10) tested a 37-wire strand of 250 ksi tensile strength under axial fatigue loading. At a stress range of 50 ksi, the first wire break occurred at 200,000 cycles. At the 75 ksi range, the first wire break occurred at 150,000 cycles.
2. Fisher and Viest (11) tested 0.192-in. wire with a strength of 257.5 ksi and a 0.375-in., 7-wire strand with a strength of 274 ksi. At a stress range of 38.4 ksi (maximum stress of approximately 200 ksi), some wires were unbroken at 2.5 million cycles, whereas at a stress range of 75.7 ksi, the fatigue life was as low as 38,000 cycles. Some wires tested at 33.5 ksi survived 7.5 million cycles. At 97.8 ksi, the fatigue life was reduced to 104,000 cycles.

Other test data could be cited that would demonstrate similar findings, but no results would deal with precisely the same wire and fretting conditions as exhibited on the I-470 Bridge.

Computed bending stresses for the first 10 modes of vibration are summarized in Table 7. Stress ranges are, of course, twice the computed stresses. Neglecting the 100 percent local stiffness values (these are shown as upper-bound stress ranges for comparison only), the seventh mode vibration of Hanger 8, the fifth and sixth modes of Hanger 5, and the fifth mode of Hanger 3, all of which were observed during the field monitoring of vibrations, correspond to stress ranges on the order of 48 to 96 ksi, 51 to 103 ksi, and 67 to 134 ksi, respectively. If 500,000 cycles is considered to be the approximate fatigue life, Strands 8, 5, and 3 would reach 500,000 cycles in only 7.9, 7.4, and 5.7 hr of vibration, respectively.

Obviously, the wind-induced strand vibration experienced on this bridge was a random loading. Modes of vibration higher than the seventh mode could have been experienced, and most certainly were experienced, under higher wind speeds than those observed during the field testing. Similarly, while the observed and computed amplitudes were in good agreement, under more uniform winds of longer duration, it is possible that higher amplitudes (and therefore stress ranges) could have been developed.

Some indication of the remaining liveload fatigue life, for those strands that have an undetectable crack as a result of fretting against the bearing plates, can be obtained by considering the number of cycles to propagate an assumed initial crack to critical crack size. Again, only limited information is available, and that is based on assumptions that did not fit the existing situation. In utilizing Equations 21-23, and the table of factors relating the crack depth, a, to the stress intensity factor, f(a), from Chi, it is possible by numerical integration to compute the theoretical number of cycles to propagate an initial crack of size a_o, to critical crack size, a_{cr}, for a given stress range, maximum stress, and fracture toughness as follows:

$$N = \int_{a_o}^{a_c} da/(0.66 \times 10^{-8})\ \Delta K^{2.25} \qquad (21)$$

where

N = number of cycles,
a_c = critical crack size,
a_o = initial crack size,
$\Delta K = \Delta\sigma\ K_1$, and
$\Delta\sigma$ = stress range.

$$K_1 = \sigma\ [(\pi a)^{1/2}]\ f(A_c/B) \qquad (22)$$

where B is the half area.

$$A_c = (\pi R^2/2) - (R-a)\ [(2aR-a^2)^{1/2}] - R^2 \tan^{-1} [(R-a)/(2aR-a^2)^{1/2}] \qquad (23)$$

The relationship between A_c/B and $f(A_c/B)$ is as follows:

A_c/B	0.1	0.2	0.3	0.4	0.5	0.6	0.7	0.8	0.9	1.0
$f(A_c/B)$	1.15	1.20	1.29	1.37	1.51	1.68	1.89	2.14	2.46	2.86

This has been done for the 0.188-in. diameter galvanized wire used in the hangers on the I-470 Bridge for assumed fracture toughness values of 60 ksi $(in.)^{1/2}$, 80 ksi $(in.)^{1/2}$, and 100 ksi $(in.)^{1/2}$ (the values assumed by Chi in his analysis of 0.25-in. diameter wire). The computed critical crack size for the higher two values of assumed fracture toughness exceeded the radius of the wire under consideration. As a practical matter, the additional number of cycles required to propagate assumed cracks from a critical crack size of 0.0837 in. [corresponding to a fracture toughness of 60 ksi $(in.)^{1/2}$ to one-half the thickness] is quite small. The following values correspond to half-thickness cracks and can be considered representative estimates of remaining fatigue life for the initial crack sizes assumed.

a_o (in.)	Cycles (million N)	
0.001	3.828	Maximum stress = 50.4 ksi
0.010	1.192	Stress range = 6.71 ksi
0.030	.390	
0.050	.139	

Traffic data given on the contract plans for the I-470 Bridge indicate average daily traffic counts of 21,800 and 31,700, respectively, for 1975 and 1995 and an estimated 7 percent truck volume. This corresponds to average daily truck traffic counts (ADTTs) of 1,526 and 2,219, respectively, for 1975 and 1995. For the discussion that follows, an average ADTT of 1,870 trucks will be used.

The maximum computed stress range is 6.71 ksi. This stress range results from 6 lanes of AASHTO lane loading, including the 75 percent, multi-lane reduction factor. Practically speaking, the lane loading is seldom realized in the field. Similarly, it is more appropriate to base fatigue considerations on the actual lane positions, rather than design positions, when trying to arrive at a more accurate estimate of fatigue life. In the case of the I-470 Bridge, if all four traffic lanes were loaded with trucks spaced at approximately 80 ft, each weighing 82 percent of the AASHTO design truck load, this would be approximately the same total weight as the six lanes of lane load at 75 percent used as the design loading. This would require 40 heavily loaded trucks to be on the bridge at one time. Obviously, the probability of this happening repeatedly during the life of the bridge is nil. Nevertheless, and only for the purpose of illustration, if the full truck traffic consisted of repetitions of this 40-truck loading, the annual ADTT would correspond to only 17,103 cycles per year. This corresponds to fatigue lives of 224, 70, 23, and 8 years for wires having assumed initial cracks of 0.001, 0.010, 0.030, and 0.050 in., respectively, at the time the bridge was put into service.

A consideration of truck loading results in even better fatigue life estimates. Based on FHWA loadometer studies, the current AASHTO fatigue specification relates the variable-amplitude loading from random truck loading to constant cycles of HS 20 design load vehicles. Basically, this results in a multiplier of 0.35 to relate ADTT to cycles of HS 20 truck loading (12). In the case of wire using a crack growth exponent of 2.25, the corresponding variable amplitude factor is 0.45. Thus, the annual ADTT of 1,870 corresponds to 843 HS 20 vehicles per day. As an illustration, if four lanes of AASHTO truck loading at 100 percent are used and if each vehicle occupies the center of its respective traffic lane, the maximum tensile stress induced in a strand is 1.5 ksi. The corresponding cycles to critical crack size for assumed initial cracks are shown in the following table. The estimated strand fatigue lives for the initial crack sizes discussed previously are then 1,450, 450, 150, and 50 years, respectively. If the two most significant of the four traffic lanes are used, resulting in twice as many cycles, virtually the same fatigue life results, as follows:

a_o (in.)	Cycles (million N)	
0.001	111.410	
0.010	34.696	Maximum stress = 50.4 ksi
0.030	11.346	Stress range = 1.50 ksi
0.050	4.035	

The discussion of remaining life has been based on several assumed configurations of the ADTT. An infinite number of other choices are possible. Obviously, many assumptions are required and the basic computational procedure is only an approximation. Nevertheless, it seems reasonable to expect that latent cracks of up to 0.03 in. will have relatively little impact on fatigue life of wires under liveload stress cycles. A latent fatigue crack of approximately 0.05 in. could be expected to have a significant effect on fatigue life only under highly improbable loadings.

CORRECTIVE ACTIONS

Recommendation

Based on the considerations outlined heretofore, recommendations were made (and eventually approved) as follows:

- Eliminate the strand vibrations through the installation of collars and strand cross ties.
- Replace only those strands with known or suspected broken wires.
- Protect lower ends of strands by means of weather-resistant enclosures.

These recommendations assume that (a) the elimination of strand vibration will eliminate the fretting potential on those original strands that are retained and that are apparently in contact with locking plates or bearing plates, and (b) some strands will crack and will have to be replaced from time to time. This latter assumption was evaluated and was found to be the cost-justified procedure.

Contract Details for Eliminating Cable Vibrations

The cable collar detail was proposed by the original designer and was based on the principle that if the uncontrolled installation of wooden wedges had effectively reduced the cable vibration, then permanent restraints should perform as well or better.

The cable collar is shown in Figure 4, and structural details thereof are shown in Figure 9. The function of the cable collar is to increase damping, and to move the fixed point away from the socket, thereby reducing bending stresses if vibrations were to continue despite the increased damping.

Details of Strand Replacement

To procedure for strand replacement involved surrounding the individual strand to be removed with a compression frame and jacking the strand to stretch it within the length of the frame. The strand to be removed could then be stretched sufficiently to free it from the attachment details. In the process, the load in that strand was transferred primarily to the other three strands in the suspender being worked on, and secondarily to other parts of the bridge. Changes in elevation along the tie member caused by bridge movement during strand replacement were barely measurable with a transit. Details of the cable removal equipment are shown in Figure 10. Note that cable grips were used to anchor the jacking force to the strand. Examination of the removed strand indicated little or no damage to individual wires resulting from the use of the cable grips. In terms of field efforts, installing the frame on each strand was the time-consuming phase of the strand replacement. This took between one and two days per installation. Jacking, relieving, and removing the strand took only a matter of minutes.

Some of the strands that were removed underwent laboratory study at Lehigh University to determine remaining fatigue resistance and to evaluate the condition of interior wires by dissection of a length of strand adjacent to a socket. Therefore, the length over which a strand was stretched was chosen to keep the strand tension below the prestretching load and within the range of linear behavior. In this manner, the strand specimen delivered to the laboratory had essentially minimized properties.

The new strands were identical to the old strands. The new top socket was also identical to the old top socket; the bottom socket was changed to a stud extension detail as shown in Figure 4. During the design phase, consideration was given to using the removal frame to stretch the new strands sufficiently for installation. This idea was rejected because, at that time, the extent of damage caused by the strand grips was not known. Once this idea was rejected, the limited working space between the suspender attachment detail and the tie girder narrowed the choice of reinstallation procedures to the use of a stud tightener. (As noted earlier, damage was found to be virtually nil during the field operations.) The stud detail also provides an effective way to tension the strand to its proper share of the suspender load because it eliminates the question of tolerance on strand length.

SUBSEQUENT DEVELOPMENTS

During the winter and early spring of 1983, the retrofit procedures described herein were undertaken. When Strand 7 DS-NW was removed, four broken wires were discovered, whereas the original inspection had indicated two suspect wires. The newly discovered broken wires were fractured approximately 0.5 in.

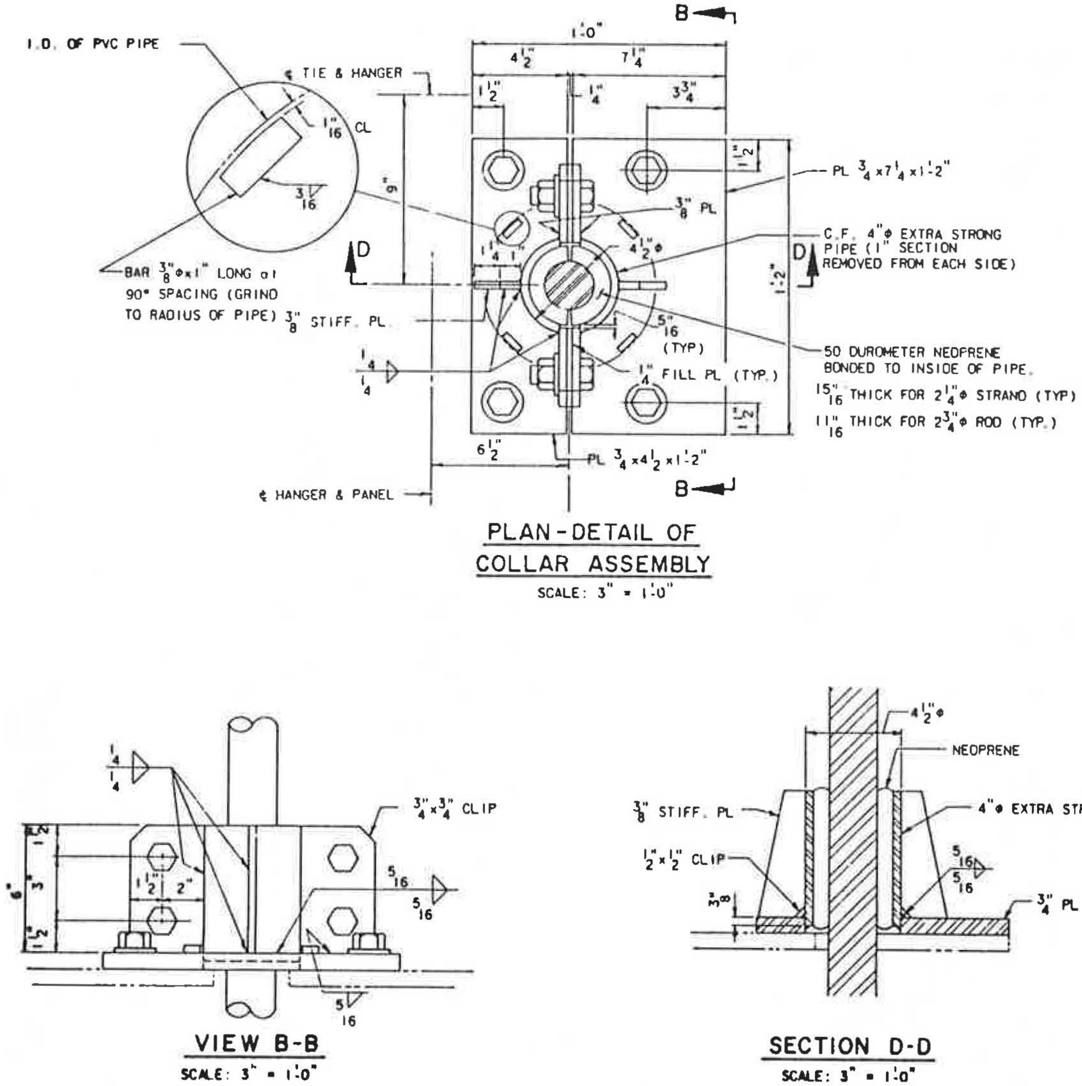

FIGURE 9 Details of cable collar.

from the socket and had therefore been held firmly in place by the bearing and locking plates of the connection detail.

The contract to replace the strands was extended to include removal and reinstallation of ten randomly selected strands. Observation of the satisfactory condition of the grip area of the originally removed strand made this procedure acceptable. In addition, another detailed visual inspection was undertaken of the tie girder and of the strands and augmented by a sounding test (hammer blow) on both ends of every exterior wire in every strand. Eight additional broken wires were discovered during the removal of 15 strands (5 original and 10 random). Four additional suspected broken wires were discovered by the soundings. Another inspection in February and March 1984 resulted in three more suspected broken wires, all at the rib end of the affected strands that had not been inspected in 1983. Plans were under way, as of December 1984, to replace the seven affected strands.

SUMMARY AND CONCLUSIONS

In this paper, a presentation has been made of a case study dealing with the investigation of the cause of broken wires in suspender strands of the I-470 Ohio River Bridge at Wheeling, West Virginia. Analytical investigation, field measurement of suspender strand vibrations, and fractographic studies of fracture surfaces led to the conclusion that vortex shedding-induced vibrations of the strands resulted in fretting fatigue where the strands were in contact with bearing plates on the weldments used to attach the suspenders to the arch tie and rib. Analytic predictions of frequencies, critical wind speeds, and amplitudes of motion were verified by field measurements.

Estimates of remaining life for partially damaged wires in the suspender strands were described for various assumed traffic configurations. Based on economic analysis of various schedules of maintenance developed from the future life estimates, decisions were made to replace selected strands that had already exhibited either known or suspected broken wires, and to maintain and service those strands that had neither confirmed nor suspected broken wires.

A technique was described by which the suspender strands were replaced. This technique is suitable on other bridges utilizing rope or bridge strand suspenders or hangers. Details of vibration dampers installed on the strands were also presented.

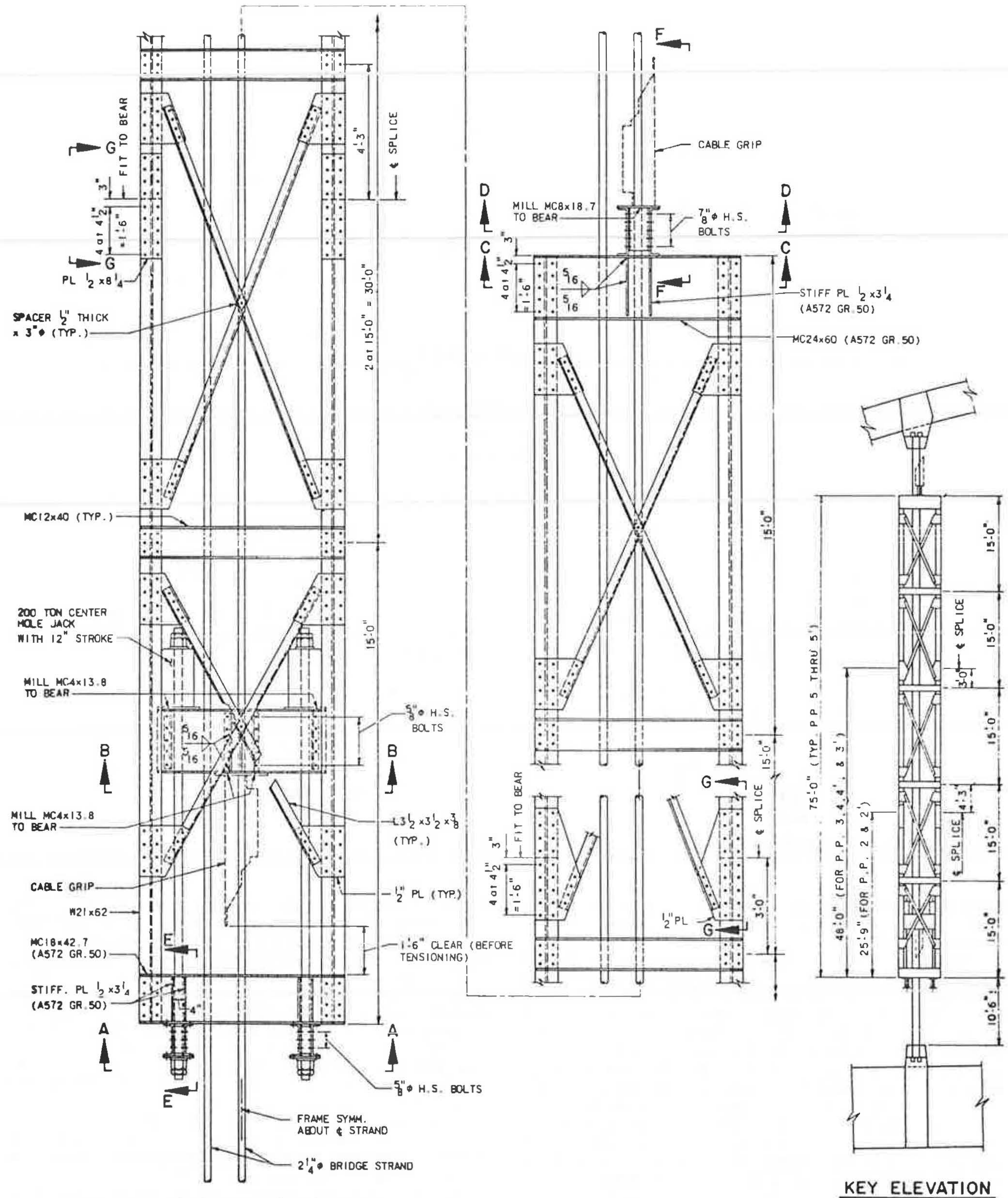

FIGURE 10 Details of cable removal equipment.

REFERENCES

1. J.W. Fisher. Observations and Findings from Examinations of Broken Wire Samples from the I-470 Bridge. Fisher, Fang, and Associates, Inc., Bethlehem, Pa., May 1981.
2. J.D. Allen and M.D. Kurre. Measurement of Natural Frequencies and Response to Wind-Induced Forces on Bridge Strands. Battelle Memorial Institute, Columbus, Ohio, May 1981.
3. M. Chi. Response of Bridge Structural Members Under Wind-Induced Vibrations. Report FHWA-RD-78-25. FHWA, U.S. Department of Transportation, June 1976.

4. M. Chi and S. Basu. Analytical Study for Fatigue of Highway Bridge Cables. Report FHWA/RD-81/090. FHWA, U.S. Department of Transportation, July 1981.
5. K. Harada et al. Aeolian Vibration of Conductor and Its Suppression Method. The Hokkaido Electric Power Company, Inc., April 1968.
6. R.A. Komenda. Wind Excitation of Stranded Cable. Preformed Line Products Company, Cleveland, Ohio, 1974.
7. H.C.S. Thom et al. Wind Forces on Structures. Paper 3269. Transactions, ASCE, Vol. 126, Part II, 1961.
8. J.M. Kulicki. Aerodynamically Induced Vibrations of H-Shapes for the Second Newburgh-Beacon Bridge (Deck Truss Spans). Modjeski and Masters, Harrisburg, Pa., April 1976.
9. R.H. Scanlan and R.L. Swart. Bending Stiffness and Strain in Stranded Cables. Conference Paper 68 CP 43-PWR. IEEE Winter Power Meeting, New York, 1968.
10. H.S. Reemsnyder. The Mechanical Behavior and Fatigue Resistance of Steel Wire, Strand, and Rope. Report of the Ad Hoc Committee on Mechanical Rope and Cable, National Materials Advisory Board, National Research Council, Washington, D.C., 1972.
11. J.W. Fisher and I.M. Viest. Fatigue Tests of Bridge Materials of The AASHO Road Test. Special Report 66, HRB, National Research Council, Washington, D.C., 1961.
12. J.W. Fisher. Bridge Fatigue Guide Design and Details. American Institute of Steel Construction, New York, 1977.

Publication of this paper sponsored by Committee on Steel Bridges.

Finite Element Analysis of Cracked Diaphragm Welds on the Ohio River Bridge at Wheeling, West Virginia

JOHN M. KULICKI, STEVEN W. MARQUISS, and RALPH J. DeSTEFANO

ABSTRACT

This paper contains a discussion on the finite element analysis of cracks in welds connecting floorbeam back-up diaphragms and web plates of box tie girders in a tied-arch bridge. Comparisons of the finite element analysis and the field instrumentation results are made at selected locations, and for one typical position of a test truck. Drawing on the conclusions of the finite element analysis, contract plans were developed to retrofit the tie girder. Two previously unconnected edges of the diaphragms were connected to the top and bottom flanges of the tie girder. Also, the floorbeam bottom flange was connected directly to the tie girder bottom flange.

Two terms are used in this paper that require definition:

- Web gap: The space left between partial-depth, tie girder diaphragms and a tie girder flange.
- Floorbeam gap: An area of incomplete or nonexistent contact between a floorbeam end plate and a tie girder web.

In March 1983, a West Virginia Department of Highways inspector made a routine inspection of the unopened, tied-arch Bridge Number 2494, which enables Interstate 470 to cross the Ohio River at Wheeling, West Virginia. A recurring pattern of weld cracking was observed during the inspection of the interior of one of the 780-ft Langer Girder arch ties. The detail involved was a fillet-welded connection of the floorbeam diaphragm and the exterior tie girder web. The interior web connection to the diaphragm was an end plate detail bolted through the tie girder web and a floorbeam end plate. Sealing diaphragms, approximately 5 ft 2 in. on each side of each floorbeam diaphragm, extended to the top and bottom tie girder flanges (no web gaps) and similar cracking was not found in these diaphragms. A Plan and Elevation view of the bridge, taken from the original designer's drawings, is shown in Figure 1 and the typical cracked diaphragm weld is shown in Figure 2.